2023 IEEE/ASME International Conference on Advanced Intelligent Mechatronics (AIM)
June 28-30, 2023. Seattle, Washington, USA

Path-following control for a slung load system

Mohamed Al Lawati Alan F. Lynch*

***Abstract*—A slung load system (SLS) is a mechanical dynamical system composed of an unmanned aerial vehicle (UAV) carrying a slung load. The nonlinear underactuated SLS dynamics make its motion control a challenging and current problem. This paper proposes a motion control that uses path-following instead of traditional trajectory-tracking. The method defines a geometric path in 3D space for the SLS to follow and renders it controlled-invariant. Output tracking error dynamics are exponentially stabilized using a dynamic state feedback linearization. Simulations demonstrate the robustness of the control to payload mass uncertainty and its benefits over trajectory-tracking.**

***Index Terms*—nonlinear control, unmanned aerial systems, slung load, path-following**

I. Introduction

Recent interest has focused on UAVs for slung load transport [1]–[4]. Such a *slung load system* (SLS) is composed of a UAV and a cable carrying a payload. This paper develops a *path-following* control (PFC) design for an SLS which ensures a subset of the configuration variables asymptotically converges to a geometric path without the need for time parameterization of the path. Key properties of the approach are that it views the path as a geometric object in 3D space and renders it controlled invariant. Typically, this objective is achieved by sending an appropriate output to zero. Moreover, a path-following problem is a generalization of a trajectory-tracking problem since a path contains a family of trajectories that correspond to it [5].

PFC arose to solve an intrinsic limitation with conventional trajectory-tracking control for linear and nonlinear systems. For linear non-minimum phase systems, when a trajectory-tracking controller is used, the work of [6] shows that there exists a fundamental limitation in transient performance where the $\mathcal{L}_2$-norm of the error is bounded from below and cannot be made arbitrarily small. The same is true for a nonlinear system with unstable zero-dynamics [7]. To address such an issue, the sequence of work [8]–[10] shows that a PFC is capable of eliminating such a performance limitation for both linear and nonlinear systems.

The literature contains two main approaches to solve a path-following problem. The first approach is pioneered by [11] and is referred to as the *maneuver regulation problem* (MRP), where the path admits a suitable parameterization. The MRP dominates path-following literature and has subsequently been studied in [5], [10], [12], [13]. With path parameterization, one can identify two control tasks

1) *a geometric task*: using the system's input, design a feedback law to drive the output to the desired parameterized path.
2) *a dynamics task*: entails controlling the time evolution of the parameterization, thus, achieving a desired velocity along the path. Here, the path parameterization is used as an additional degree of freedom and is given a temporal reference signal to track.

This technique has been applied to control systems with unstable zero-dynamics. For example, the work of [12] formulates an MRP for a planar vertical takeoff and landing (P-VTOL) aircraft. To stabilize unstable-zero dynamics for a general nonlinear system, the work of [5], which is based on the sequence of results [8], [9], [14], designs a suitable timing law for the path parameterization. With unknown time-varying bounded disturbances, robust PFC is studied in [13] by careful assignment of path parameterization dynamics. Robustness to parametric uncertainty in underactuated vehicles is addressed in [15] using adaptive switching supervisory control, and a comparison with trajectory-tracking is presented. Note that, in all aforementioned work, the dynamic task is still achieved by solving a conventional trajectory-tracking problem for the path parameterization, and hence, has the shortcomings of trajectory-tracking. To avoid tracking a timed signal within the dynamic task, one may resort to set stabilization. Within this framework, virtual holonomic constraints (VHC) have been used in [16] to solve a path-following problem for underactuated nonlinear systems. VHCs have also been applied to mechanical systems [17], [18]. Furthermore, passivity has been used to accomplish path invariance for the unicycle [19] for circular paths. Another set stabilization approach establishes a transformation that decomposes the system dynamics into two components relative to the path: transverse and tangential. The corresponding feedback exploits this decomposition and leads to the concept of transverse feedback linearization (TFL). Early results in this framework include [20], [21]. The work of [22] uses TFL to stabilize periodic orbits for single-input nonlinear systems. Subsequently, further development appeared in [23] for multi-input Euler-Lagrange mechanical systems, where instead of using the rank of the decoupling matrix, certain necessary and sufficient conditions are imposed on the output function so that the system has a well-defined relative degree of $\{2, \ldots, 2\}$, thus, allowing for TFL. It is interesting to note that, besides being viewed as an example of an MRP [12], the P-VTOL was also studied as an instance

This work is funded by Sultan Qaboos University (SQU), Oman, and the Natural Sciences and Engineering Research Council (NSERC) of Canada.

M. Al Lawati and A.F. Lynch are with the Department of Electrical and Computer Engineering at the University of Alberta, Canada.

M. Al Lawati is also with the Department of Mechanical and Industrial Engineering, Sultan Qaboos University, Oman.

* Corresponding author. Email: alan.lynch@ualberta.ca

of a TFL problem in [24].

Within research on SLS motion control, path following with a set stabilization framework has gained recent attention. The work of [25] addresses the problem of following straight lines using Reduction Theorems of [26]. Curved paths are approximated with lines, and therefore, controller switching is inevitable. The work of [27] allows for smooth curved paths. However, the controller design is based on constant cable tension, which is taken to equal the weight of the payload. This assumption is unrealistic. The contributions of this paper are twofold. We design a PFC addressing the limitations of both [25] and [27]. In particular, unlike [25], our control law is a smooth function of the state vector and achieves path-following for any smooth Jordan curve. Hence, no switching is required and a simple exponential stability property for the error dynamics results. Also, in contrast to [27], our design does not assume constant cable tension. Rather, tension is a function of state. We follow the set stabilization approach and use dynamic state feedback linearization.

Notation: Let $f : \mathbb{R}^n \to \mathbb{R}^n$ denote a vector-valued function and $g : \mathbb{R}^n \to \mathbb{R}$ is a scalar function. The Lie derivative of g along f is denoted $L_f g$. The gradient of f with respect to $x \in \mathbb{R}^n$ is $\mathrm{d}_x f$. The components of x are denoted as $x_1, \ldots, x_n$. The $(i,j)^{\text{th}}$ entry of a matrix J is $J_{i,j}$. We abbreviate $\sin\varphi$, $\cos\varphi$ and $\tan\varphi$ as s_φ, c_φ, and t_φ, respectively. Given vectors $a_1, \ldots, a_n$, the column vector composed by concatenating $a_1, \ldots, a_n$ is denoted $\mathrm{col}(a_1, \ldots, a_n)$. The $n \times m$ zero matrix is $0_{n\times m}$, and the $n \times n$ identity matrix is I_n.

II. Dynamic Model

This paper investigates motion control for a so-called *slung load system* (SLS) shown in Fig. 1. The SLS consists of a UAV carrying a simple pendulum consisting of a massless rod carrying a point mass payload m_L. The massless rod is attached to the UAV's center of mass (CoM) and can rotate with 2 DoF (degrees of freedom). We define an

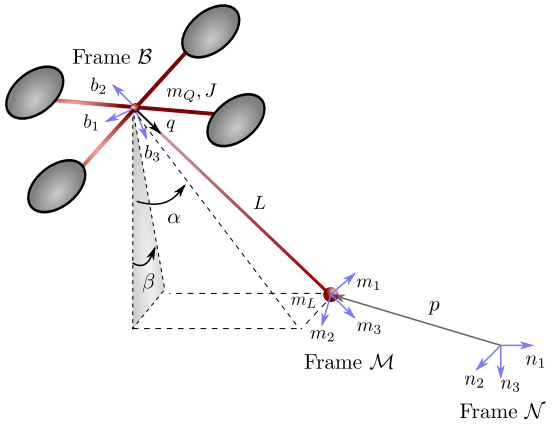

Fig. 1: The SLS showing configuration variables and parameters.

inertial frame $\mathcal{N} = (n_1, n_2, n_3)$ and two moving frames $\mathcal{B} = (b_1, b_2, b_3), \mathcal{M} = (m_1, m_2, m_3)$. Frame $\mathcal{B}$ is fixed to the UAV's CoM and $\mathcal{M}$ is attached to m_p. We orient $\mathcal{B}$ such that b_3 points down, and b_1 points in the vehicle's forward direction. The UAV propellers are assumed to generate thrust in the $-b_3$ direction. The frame $\mathcal{M}$ is located at m_L and oriented such that m_3 is along the unit direction vector of the pendulum q. We define $p \in \mathbb{R}^3$ as the position of the origin of $\mathcal{M}$ with respect to $\mathcal{N}$. The pendulum's orientation is described by $\eta_p = \mathrm{col}(\alpha, \beta) \in \mathbb{R}^2$. Frame $\mathcal{M}$ is rotated by angle α about n_1 and angle β about n_2.

Turning to the UAV rotational dynamics, we define $\eta_q = \mathrm{col}(\phi, \theta, \psi) \in \mathbb{R}^3$ which are 2-1-3 Euler angles parameterizing the relative orientation between $\mathcal{B}$ and $\mathcal{N}$. We chose 2-1-3 Euler angles since they yield simpler model and control law expressions. We define angular rates $\gamma_p = \mathrm{col}(\dot\alpha, \dot\beta)$ and $\gamma_q = \mathrm{col}(\dot\phi, \dot\theta, \dot\psi)$. Hence, defining ω_q as the UAV angular velocity, we have $\gamma_q = W(\eta_q)\omega_q$, where

$$W(\eta_q) = \begin{bmatrix} \mathrm{s}_\psi/\mathrm{c}_\phi & \mathrm{c}_\psi/\mathrm{c}_\phi & 0 \\ \mathrm{c}_\psi & -\mathrm{s}_\psi & 0 \\ \mathrm{t}_\phi\mathrm{s}_\psi & \mathrm{t}_\phi\mathrm{c}_\psi & 1 \end{bmatrix}.$$

Using the Euler-Lagrange Equations (see [28] for related background), the dynamics of the SLS are

$$\dot x = f(x) + G(x)u, \text{ where}$$

$$f(x) = \begin{bmatrix} v \\ \gamma_p \\ W(\eta_q)\omega_q \\ a\left\|\mathrm{d}_{\eta_p} q \cdot \gamma_p\right\|^2 q + g e_3 \\ 2\mathrm{t}_\beta \gamma_\alpha \gamma_\beta \\ -\mathrm{s}_\beta \mathrm{c}_\beta \gamma_\alpha^2 \\ J^{-1}\left(J\omega_q \times \omega_q\right) \end{bmatrix}, G(x) = \begin{bmatrix} 0_{8\times 1} & 0_{8\times 3} \\ -\frac{(q\cdot b_3)q}{M} & 0_{3\times 3} \\ -\frac{m_2 \cdot b_3}{L m_Q \mathrm{c}_\beta} & 0 \\ \frac{m_1 \cdot b_3}{L m_Q} & 0 \\ 0_{3\times 1} & J^{-1} \end{bmatrix}, \tag{1}$$

where $e_3 = \mathrm{col}(0,0,1)$, $x = \mathrm{col}(x_q, x_v) \in \mathbb{R}^{16}$, the SLS configuration variable is $x_q = \mathrm{col}(p, \eta_p, \eta_q) \in \mathbb{R}^8$, $x_v = \mathrm{col}(v, \gamma_p, \omega_q) \in \mathbb{R}^8$, $v = \dot p$. The input for (1) is $u = \mathrm{col}(T, \tau) \in \mathbb{R}^4$ where $T \in \mathbb{R}$ is total propeller thrust, and $\tau \in \mathbb{R}^3$ is propeller torque applied to the UAV and expressed in $\mathcal{B}$. The payload mass is m_L, the UAV mass is m_Q. We define $M = m_Q + m_L$ and $a = -Lm_Q/M$. The UAV inertia matrix is $J = \mathrm{diag}\,(J_{1,1}, J_{2,2}, J_{3,3}) \in \mathbb{R}^{3\times 3}$, pendulum length is L, and the gravitational constant is g.

Clearly model (1) is undefined whenever $\mathrm{c}_\beta = 0$ or $\mathrm{c}_\phi = 0$. Thus, the state space $\mathcal{X}$ of the SLS is the subset of $\mathbb{R}^{16}$ excluding these points.

III. Problem Description

This paper presents a PFC for an SLS described by (1). Note that, unlike a trajectory-tracking design, the path object in PFC is not parametrized by time. Rather, the path is a geometric curve in 3D space and desired payload position is independent of time. For practical reasons, the PFC should be robust to model uncertainty, and we focus on unknown payload mass m_L.

To define the desired path we consider a Jordan curve in $\mathbb{R}^3$, i.e., a smooth closed curve without self-crossings. Such a

curve $\mathcal{C}$ can be written as the intersection of two surfaces in $\mathbb{R}^3$

$$\mathcal{C} = \{p \in \mathbb{R}^3 : h_1(p) = 0, h_2(p) = 0\}. \tag{2}$$

where $h_1(p) = 0$ and $h_2(p) = 0$ are surfaces. Note that since $\mathcal{C}$ is a Jordan curve, at every $p \in \mathcal{C}$ the tangent vector ρ is well-defined and is given by

$$\rho(p) = \frac{\mathrm{d}_p h_1(p) \times \mathrm{d}_p h_2(p)}{\|\mathrm{d}_p h_1(p) \times \mathrm{d}_p h_2(p)\|}. \tag{3}$$

The PFC has the following goals:

- **G1** The payload position exponentially converges to $\mathcal{C}$.
- **G2** The payload velocity exponentially converges to a desired velocity profile specified on $\mathcal{C}$.
- **G3** The UAV yaw exponentially converges to a desired profile specified on $\mathcal{C}$.
- **G4** Goals **G1–G3** should be achieved without knowing m_L.

We view **G1** as the primary control objective, while **G2 –G3** are secondary goals.

We remark that the geometric shape of a path $\mathcal{C}$ can be tracked using a conventional trajectory-tracking controller, e.g., [29]. However, PFC has the following advantages.

- **A1** A PFC renders the geometric path $\mathcal{C}$ controlled invariant [30].
- **A2** A path $\mathcal{C}$ is associated with a family of timed reference trajectories [5]. Hence, transient performance of a trajectory-tracking design depends on the specific reference chosen. However, PFC does not suffer from this dependence. This leads to smoother and more natural transients since the error is defined as a deviation from a geometric path and not a timed reference signal.

The benefits of property **A1** can arise in the following cases:

- When the system is initialized on $\mathcal{C}$, PFC will keep it there independent of intial velocity. For trajectory-tracking, initial velocity has to match the reference value for the system to remain on the reference.
- Suppose a system moves on $\mathcal{C}$. Suppose that an external influence suddenly brings the system to rest. After this influence is removed, a PFC ensures motion will continue along $\mathcal{C}$ without leaving it. However, with trajectory-tracking design, the system generally moves away from the path as it attempts to catch up with the timed reference trajectory. This leads to undesirable transient performance.

Property **A1** can only be achieved by solving a set stabilization problem and not an MRP since the dynamic task of an MRP requires solving a trajectory-tracking problem. Property **A2** is not restricted to any particular PFC approach. For example, the improved transient performance in an MRP framework is discussed in [15].

IV. SLS Path-Following Control (PFC)

To achieve the goals **G1–G4** we follow an output stabilization approach with output

$$h(p, v, \psi) = \begin{bmatrix} h_1(p) \\ h_2(p) \\ \rho(p) \cdot v - v_{\mathrm{d}}(p) \\ \psi - \psi_{\mathrm{d}}(p) \end{bmatrix}, \tag{4}$$

where $v_{\mathrm{d}} : \mathbb{R}^3 \to \mathbb{R}$ is the desired velocity profile of the payload on $\mathcal{C}$, and $\psi_{\mathrm{d}} : \mathbb{R}^3 \to \mathbb{R}$ is desired UAV yaw on $\mathcal{C}$.

To null (4), we use input-output feedback linearization. We remark dynamics (1) with output (4) is not statically input-output state feedback linearizable since its relative degree is not well-defined. To see this, we take time-derivatives of each output component until the first input appears. We obtain a singular decoupling matrix

$$A(x) = \begin{bmatrix} -\epsilon(\mathrm{d}_p h_1 \cdot q) & 0 & 0 & 0 \\ -\epsilon(\mathrm{d}_p h_2 \cdot q) & 0 & 0 & 0 \\ -\epsilon(\mathrm{d}_v h_3 \cdot q) & 0 & 0 & 0 \\ -\epsilon(\mathrm{d}_p \psi_d \cdot q) & \frac{W_{3,1}}{J_{1,1}} & \frac{W_{3,2}}{J_{2,2}} & \frac{W_{3,2}}{J_{3,3}} \end{bmatrix}, \tag{5}$$

where $\epsilon = q \cdot b_3/M$, and $W_{i,j}$ is the (i,j)th entry of W.

However, we can dynamically extend (1) to achieve a input-output state feedback linearization. This approach delays the appearance of thrust in time derivatives of the output until relative degree becomes well-defined. During dynamic extension, input τ is not transformed. It turns out we must take four time-derivatives of the output until we get a well-defined relative degree. Based on the above, we define a new state ζ_1 to be the vertical component of payload acceleration. In other words

$$\zeta_1 = \dot{v}_3. \tag{6}$$

Furthermore, we define three additional states as $\zeta_{i+1} = \dot{\zeta}_i, i = 1, 2, 3$. Let the *controller state* be $\zeta = \mathrm{col}(\zeta_1, \zeta_2, \zeta_3, \zeta_4) \in \mathbb{R}^4$. Hence, the controller dynamics becomes

$$\dot{\zeta}_1 = \zeta_2,\ \dot{\zeta}_2 = \zeta_3,\ \dot{\zeta}_3 = \zeta_4,\ \dot{\zeta}_4 = u_\zeta, \tag{7}$$

where $u_\zeta \in \mathbb{R}$ is a new control input. Defining an extended state vector $\bar{x} = \mathrm{col}(x, \zeta) \in \mathbb{R}^{20}$ and a new input vector $\bar{u} = \mathrm{col}(u_\zeta, \tau) \in \mathbb{R}^4$, the extended SLS dynamics becomes

$$\dot{\bar{x}} = \bar{f}(\bar{x}) + \bar{G}(\bar{x})\bar{u}, \tag{8}$$

where $\bar{f} : \mathbb{R}^{20} \mapsto \mathbb{R}^{20}$ and $\bar{G} : \mathbb{R}^{20} \mapsto \mathbb{R}^{20\times 4}$. Their expressions are lengthy and omitted for brevity. We remark that the thrust of the original SLS (1) becomes

$$T = \frac{M}{(q \cdot e_3)(q \cdot b_3)} \left(f_{11} - \zeta_1\right). \tag{9}$$

By direct computation of the decoupling matrix, system (8) with output (4) achieves a well-defined relative degree of $\{r_1, r_2, r_3, r_4\} = \{6, 6, 5, 2\}$ on $\mathcal{C}$ if and only if (1) the pendulum is not perpendicular to the direction of thrust, (2) thrust remains positive, (3) the payload does not accelerate at a rate of g downwards, and (4) $\alpha \neq \pm\frac{\pi}{2}$. To see this, consider the following reasoning.

The numerator of the determinant of the decoupling matrix is

$$m_Q L M^2 (b_3 \cdot q) \mathrm{d}_\psi h_4 (\zeta_1 - f_{11})^2 (\zeta_1 - g)^2 (\mathrm{d}_p h_1 \times \mathrm{d}_p h_2) \cdot \mathrm{d}_v h_3.$$

From (3), we have $\mathrm{d}_p h_1 \times \mathrm{d}_p h_2 = \rho \, \|\mathrm{d}_p h_1 \times \mathrm{d}_p h_2\|$. In addition, we have $\mathrm{d}_v h_3 = \rho$ (see (4)). Therefore, since ρ is a unit vector, we get $(\mathrm{d}_p h_1 \times \mathrm{d}_p h_2) \cdot \mathrm{d}_v h_3 = (\rho \cdot \rho) \, \|\mathrm{d}_p h_1 \times \mathrm{d}_p h_2\| = \|\mathrm{d}_p h_1 \times \mathrm{d}_p h_2\| \neq 0$ since $\mathrm{d}_p h_1 \times \mathrm{d}_p h_2 \neq 0$ by construction of the path $\mathcal{C}$. As for $\mathrm{d}_\psi h_4$, it is evident by the definition of h_4 in (4) that $\mathrm{d}_\psi h_4 \equiv 1 \neq 0$. Whenever $b_3 \cdot q = 0$, this corresponds to the pendulum being perpendicular with the thrust direction by the definitions of b_3 and q. Also, $\zeta_1 - f_{11} = 0$ corresponds to $T = 0$ (see (9)). When $\zeta_1 - g = 0$ holds, it is clear that whenever the vertical acceleration of the payload is g, the determinant of the decoupling matrix becomes zero. The denominator of the determinant of the decoupling matrix is

$$(L m_Q)^2 J_{1,1} J_{2,2} J_{3,3} \left(\cos(\alpha)\cos(\beta)\right)^5 \kappa(\alpha, \beta, \phi, \theta),$$

where the expression for $\kappa(\alpha, \beta, \phi, \theta)$ is to large to present. It can be shown that $\kappa \neq 0$ when $\beta, \alpha \neq \pm\pi/2$. Thus, the denominator of determinant becomes zero when $\cos\alpha = 0$ or $\cos\beta = 0$. Note that the latter point is a model singularity and has been excluded from the state space. The above reasoning implies a well-defined relative degree on $\mathcal{C}$.

The above singularity conditions represent aggressive maneuvers not encountered during safe flight. The path $\mathcal{C}$ should be designed so that the motion along $\mathcal{C}$ does not encounter such points. Intuitively, a path with sufficiently low desired tangential velocity and low path curvature stays away from such unsafe conditions. This imposes upper bound restrictions on these two quantities. We will consider paths with such characteristics throughout the paper. We remark that in [31], an upper bound on path curvature is also required for the PFC of a P-VTOL.

Notice that, for system (8), (4), the path-following problem can be viewed as the problem of stabilizing the zero-dynamic manifold $\mathcal{Z}$:

$$\mathcal{Z} = \{\bar{x} \in \mathbb{R}^{20} : L_{\bar{f}}^j h_i, j = 0, \ldots, r_i - 1, i = 1, \ldots, 4\}. \quad (10)$$

We remark that $\mathcal{Z}$ can be interpreted as the set containing all possible motions of the SLS that ensures the payload position is in $\mathcal{C}$ using an appropriate feedback.

A. Path-following control (PFC) design

Since $\{r_1, r_2, r_3, r_4\} = \{6, 6, 5, 2\}$ on $\mathcal{C}$, continuity implies that this also holds in a neighborhood of $\mathcal{C}$. We define $\bar{b} = \mathrm{col}(L_{\bar{f}}^{r_1} h_1, L_{\bar{f}}^{r_2} h_2, L_{\bar{f}}^{r_3} h_3, L_{\bar{f}}^{r_4} h_4)$ and denote the decoupling matrix as $\bar{A}$, we design a linearizing controller for (8) as

$$\bar{u} = \bar{A}^{-1}(-\bar{b} + \nu), \quad (11)$$

where $\nu \in \mathbb{R}^4$ is the auxiliary control input. Notice that after applying (11) to (8), the zerodynamics are 1-dimensional. Also, the zero dynamics evolve on the path $\mathcal{C}$, which is diffeomorphic to a unit circle $\mathbb{S}^1$. Therefore, the path is a compact set implying the zero dynamics do not affect the stability of the error dynamics. This fact is formally proved in [32].

To write the system in a canonical form, let $(\xi, \eta) \in \mathbb{R}^{20}$ where $\xi \in \mathbb{R}^{19}$ represents the state of the error dynamics, and $\eta \in \mathbb{R}$ is the zero dynamics state. Now, consider the following coordinate transformation

$$\mathrm{col}(\xi \vdots \eta) = \sigma(\bar{x}) = \mathrm{col}(\xi^1(\bar{x}), \xi^2(\bar{x}), \xi^3(\bar{x}), \xi^4(\bar{x}) \vdots \eta(\bar{x})),$$

where, for $i = 1, 2, 3, 4$, we have

$$\xi^i = \mathrm{col}\left(h_i(\bar{x}), L_{\bar{f}} h_i(\bar{x}), \ldots, L_{\bar{f}}^{r_i} h_i(\bar{x})\right).$$

Thus, the ξ-dynamics can be written as

$$\dot{\xi} = A_c \xi + B_c \nu, \quad (12)$$

where

$$A_c = \begin{bmatrix} A_{c_1} & \cdots & 0 \\ \vdots & \ddots & \vdots \\ 0 & \cdots & A_{c_4} \end{bmatrix}, B_c = \begin{bmatrix} B_{c_1} & \cdots & 0 \\ \vdots & \ddots & \vdots \\ 0 & \cdots & B_{c_4}, \end{bmatrix}$$

and for $i = 1, 2, 3, 4$, we have the following Brunovsky pairs

$$A_{c_i} = \begin{bmatrix} 0 & I_{(r_i - 1)} \\ 0 & 0 \end{bmatrix} \in \mathbb{R}^{r_i \times r_i} \text{ and } B_{c_i} = \begin{bmatrix} 0 \\ 1 \end{bmatrix} \in \mathbb{R}^{r_i}.$$

The ξ-dynamics can be made exponentially stable by the feedback

$$\nu = -K\xi, \quad (13)$$

where $K \in \mathbb{R}^{4 \times 19}$ stabilizes the origin of the ξ-dynamics. Since the η-dynamics do not affect the stability of the ξ-dynamics as discussed above, the objectives **G1–G3** are achieved.

B. Disturbance compensation

To add robustness to the PFC, we augment the controller (11), (13) with integral action, which is capable of eliminating constant steady-state error [33]. Let $\tilde{\xi} = \int_0^t h(\bar{t}) \mathrm{d}\bar{t}$ represent the integral error state. Therefore, the error dynamics is

$$\dot{\xi} = A_c \xi + B_c \tilde{\nu} \quad (14a)$$

$$\dot{\tilde{\xi}} = \mathrm{col}(\xi_1, \xi_7, \xi_{13}), \quad (14b)$$

To stabilize (14), we use the auxiliary control

$$\tilde{\nu} = \nu - \mathrm{col}(\tilde{K}\tilde{\xi}, 0), \quad (15)$$

where $\tilde{K} \in \mathbb{R}^{3 \times 3}$ is a diagonal matrix with positive entries. The gains K and $\tilde{K}$ exponentially stabilize the origin of (14).

V. Circular path example

Here, we consider the path to be a horizontal circle in 3D space with radius d_1 located at a height of d_2 The corresponding path is $\mathcal{C} = \{p \in \mathbb{R}^3 : p_1^2 + p_2^2 - d_1 = 0, p_3 - d_2 = 0\}$. Taking $\psi_\mathrm{d} = 0$, the output function is

$$h(p, v, \psi) = \begin{bmatrix} p_1^2 + p_2^2 - d_1^2 \\ p_3 - d_2 \\ \frac{p_1 v_2 - p_2 v_1}{\sqrt{p_1^2 + p_2^2}} - v_\mathrm{d} \\ \psi \end{bmatrix}. \tag{16}$$

We choose $d_1 = 5\,\mathrm{m}$, $d_2 = -10\,\mathrm{m}$. The proposed control design is applied to an SLS whose parameters are shown in Table I. With our PFC, Fig. 2 highlights the advantage **A1**. In

TABLE I: SLS parameters used to study a circular path.

m_L	$0.5\,\mathrm{kg}$
m_Q	$2.5\,\mathrm{kg}$
$J_{1,1}$	$0.03\,\mathrm{kg{\cdot}m^2}$
$J_{2,2}$	$0.03\,\mathrm{kg{\cdot}m^2}$
$J_{3,3}$	$0.05\,\mathrm{kg{\cdot}m^2}$
L	$2\,\mathrm{m}$

particular, Fig. 2a illustrates a path-following scenario while Fig. 2b presents a trajectory-tracking framework, in which the output is taken as $y(t) = \mathrm{col}(p, \psi) \in \mathbb{R}^4$ and the reference output is set to $y^{\mathrm{ref}}(t) = \mathrm{col}(d_1 \sin(t), d_1 \cos(t), d_2, 0)$ so the payload tracks the same circle. Both scenarios initialize the SLS at the same point of $\mathcal{C}$. At the beginning of the motion, both controllers perform equally well in terms of staying on the desired path/trajectory. However, when an obstacle stops the SLS suddenly while resetting the pendulum to the downward orientation and the UAV to horizontal orientation, the PFC does not cause the SLS to leave its path after the obstacle has been removed. The trajectory-tracking controller, on the other hand, has undesirable transient performance as it catches up with the timed reference.

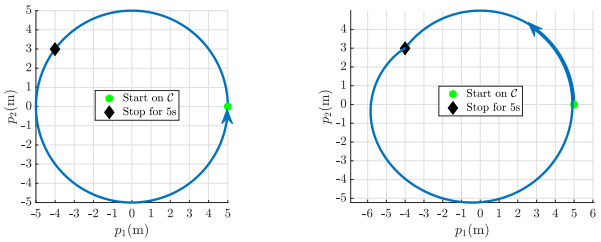

(a) PFC. (b) Trajectory-tracking.

Fig. 2: Path invariance benefits of PFC versus trajectory-tracking.

Turning to **A2**, it is obvious that for $\varphi, \varepsilon \in \mathbb{R}$ and $k \in \mathbb{N}$, the family of trajectories $\mathcal{Y}^{\mathrm{ref}} = \mathrm{col}\left(d_1 \sin(\varepsilon t + \varphi), d_1 \sin(\varepsilon t + \varphi + (2k-1)\pi/2), d_2\right)$ are contained in a single geometric circular path $\mathcal{C}$. Different choices for the parameters yield different transient behaviours. In our choice of y^{ref}, we have $\varepsilon = 1$, $\varphi = 0$ and $k = 1$. Fig. 3 highlights the improved transient performance of the proposed PFC. To meet **G1**–**G3**, we select the gain matrix K such that the eigenvalues of the ξ^1, ξ^2-subsystems are -2 and the eigenvalues ξ^3, ξ^4-subsystems are -1. For the trajectory-tracking control design, we locate the eigenvalues of the error dynamics of y_1, y_2 and y_3 at -1.5 and the eigenvalues of the error dynamics of y_4 at -1. In both scenarios, the SLS is initialized at rest outside the circle at $p(0) = \mathrm{col}(0, 9, -10)\mathrm{m}$ with pendulum pointing "downwards", i.e $\alpha = \beta = 0$. It is obvious from Fig. 3a that the PFC leads the payload to its *geometric path* in a "smarter" way than a trajectory-tracking controller (Fig. 3b), which takes the payload to its desired *timed reference trajectory*. The improved transients of the PFC can be quantified using two measures: (i) the point-to-set distance metric given by $d_{\mathcal{C}} = \inf_{p^* \in \mathcal{C}} \|p - p^*\|$, and (ii) the control effort exerted during transient, which can be quantified using $\|u(t)\|$. For the circular path at constant height described by the first two components of (16), the closest point $p^* \in \mathcal{C}$ to p can be described as $\mathrm{col}(p_1^*, p_2^*) = d_1 \left(\frac{\mathrm{col}(p_1, p_2)}{\|\mathrm{col}(p_1, p_2)\|}\right)$ and $p_3^* = d_2$. Fig. 4 compares the performance of PFC with trajectory-tracking. It is clear that while the PFC moves the payload to its path $\mathcal{C}$ in a smoother and faster way, it uses less control effort during transient.

Although we have argued the zero dynamics do not make the system unstable, it is worth discussing the motion on $\mathcal{Z}$, which is represented by the evolution of η. To identify η, let $\eta = s(p)$, where $s(p)$ is the arc-length of the circle $\mathcal{C}$ measured counterclockwise (CCW) from the positive p_1-axis. Also, let $\vartheta \in [-\pi, \pi]$ represent the angle measured CCW from the positive p_1-axis. Then, for a point on the circle, we have

$$s = d_1 \vartheta. \tag{17}$$

Noting that $\tan\vartheta = p_2/p_1$, we conclude the Jacobian of the transformation $\sigma(\bar{x})$ is full rank Hence, s serves as a valid choice for η. Therefore, the dynamics on $\mathcal{Z}$ can be easily written as

$$\dot{s} = v_\mathrm{d}. \tag{18}$$

We remark that since v_d is a design parameter, it can be viewed as an additional virtual input that controls the motion on $\mathcal{Z}$.

We now discuss goal **G4**. Suppose the PFC uses a nominal value of payload mass $\tilde{m}_p$ which is not accurate. For this case, the integral action (14), (15) eliminates steady-state error. When $\tilde{m}_L < m_L$ (respectively, $\tilde{m}_L > m_L$), the payload converges to a circle with larger (respectively, smaller) radius $\tilde{d}_1$ at a lower (respectively, higher) elevation $\tilde{d}_2$ with tangential velocity $\tilde{v}_\mathrm{d}$ being higher (respectively, lower) than v_d. The disturbance does not affect the UAV yaw dynamics. Figs. 5 and 6 illustrate this phenomenon. In Fig. 5, we take $\tilde{m}_L = 0.25\,\mathrm{kg}$, whereas in Fig. 6, $\tilde{m}_L = 0.75\,\mathrm{kg}$. The actual payload mass is in Table I. Both figures compare output trajectories with and without integral action, and show snapshots of the SLS when the integral action is active. It is clear from Fig. 5a that the absence of integral action causes the payload to eventually traverse a circle with a larger radius at a lower height. Similarly, Fig. 6a shows that in steady-state,

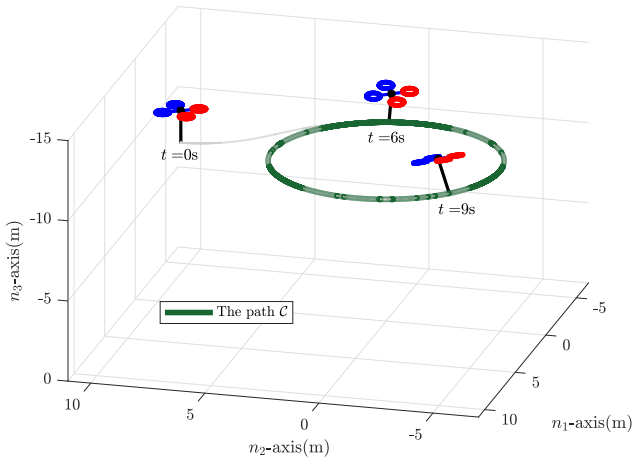

(a) PFC.

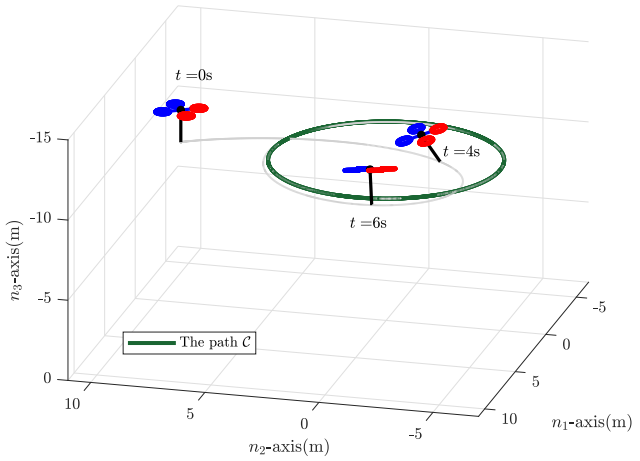

(b) Trajectory-tracking.

Fig. 3: Comparing transient performance of PFC and trajectory-tracking.

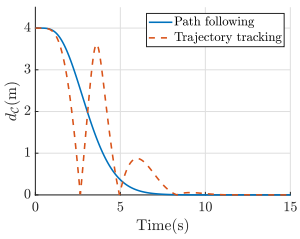

(a) Distance $d_{\mathcal{C}}$ for PFC and trajectory tracking.

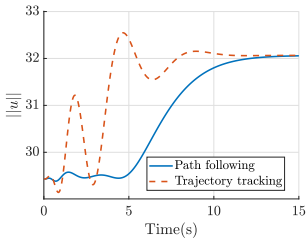

(b) Controller effort $\|u\|$ for PFC and trajectory tracking.

Fig. 4: Performance comparison of PFC and trajectory-tracking.

the payload converges to a circular path with smaller radius at a increased height.

The initial conditions are taken as $p(0) = \text{col}(5, 4, -2)\text{m}$, $v(0) = \text{col}(0.1, -0.1, 0.2)\text{m/s}$, $\eta_p(0) = \text{col}(\pi/9, 0)\text{rad}$, $\gamma_p(0) = \text{col}(-0.01, 0)\text{rad/s}$, $\eta_q(0) = \text{col}(\pi/18, -\pi/9, 2\pi/9)\text{rad}$ and $\gamma_q = \text{col}(0, 0.1, -0.2)\text{rad/s}$. The controller state is initialized at $\zeta(0) = \text{col}(-g, 0, 0, 0)$. The controller gain K was set so that the eigenvalues of the ξ^1 and ξ^2 subsystems located at $\{-1, -2, -3, -4, -5, -6\}$, the eigenvalues of the ξ^3 subsystem located at $\{-1, -2, -3, -4, -5\}$ and the eigenvalues of the ξ^4 subsystem located at $\{-1, -2\}$. The integral gain matrix $\tilde{K}$ was set to $\tilde{K} = \text{diag}(120, 100, 40)$.

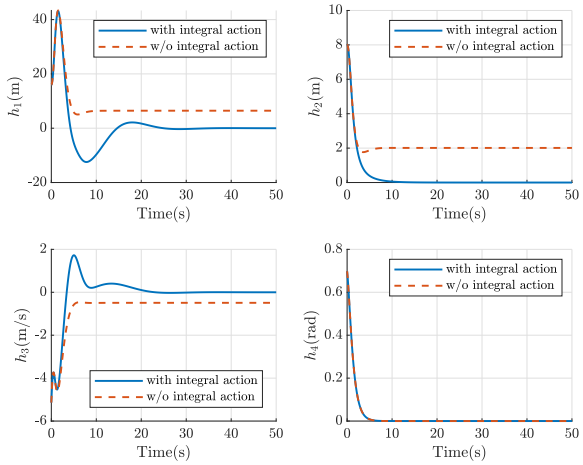

(a) Output plots without integral action (using auxiliary control (13)) and with integral action (using auxiliary control (15)).

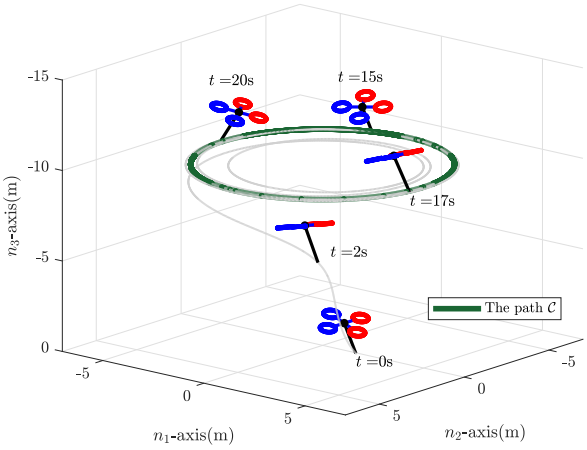

(b) Snapshots of the SLS using auxiliary control (15).

Fig. 5: Integral control is capable of rejecting payload mass disturbance when the SLS picks a heavier mass.

VI. Conclusion

This paper addressed the motion control problem of an SLS. The proposed method uses a path-following framework. The control objective includes path following of the payload mass position with a prescribed velocity and UAV yaw. Since

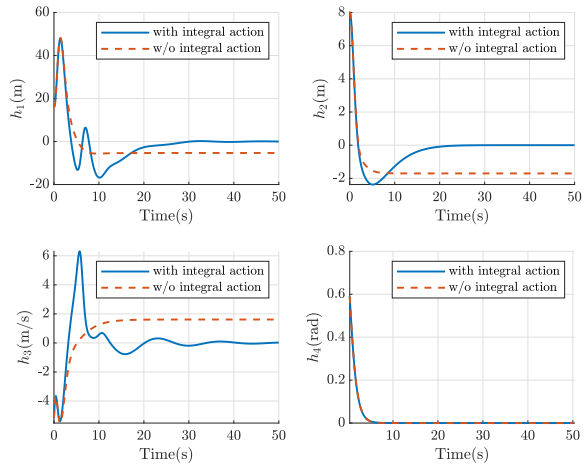

(a) Output plots without integral action (using auxiliary control (13)) and with integral action (using auxiliary control (15)).

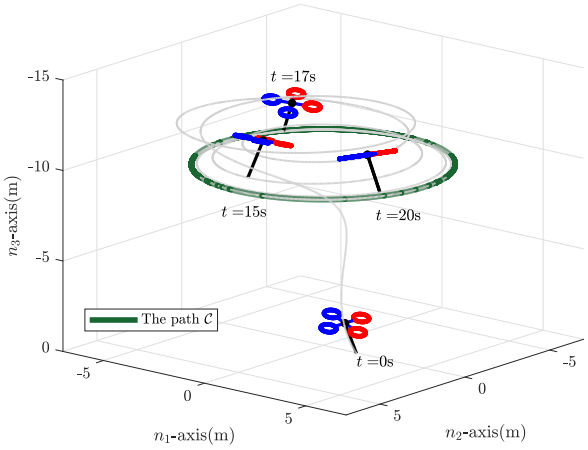

(b) Snapshots of the SLS using auxiliary control (15).

Fig. 6: Integral control is capable of rejecting payload mass disturbance when the SLS picks a lighter mass.

the SLS does not possess a well-defined relative degree we apply dynamic state feedback linearization to obtain a simpler error dynamics stability proof. Integral augmentation provides robustness to payload mass uncertainty as shown in numerical simulation. The benefits of path following over conventional trajectory-tracking are shown.

REFERENCES

[1] K. Sreenath, T. Lee, and V. Kumar, "Geometric control and differential flatness of a quadrotor UAV with a cable-suspended load," in *Proc. IEEE Int. Conf. on Decision and Control*, Dec 2013.

[2] M. M. Nicotra, E. Garone, R. Naldi, and L. Marconi, "Nested saturation control of an UAV carrying a suspended load," in *Proc. American Control Conf.*, 2014, pp. 3585–3590.

[3] K. Klausen, T. I. Fossen, and T. A. Johansen, "Nonlinear control with swing damping of a multirotor UAV with suspended load," *J. Intell. Robot. Syst.*, vol. 88, no. 2, pp. 379–394, 2017.

[4] D. Cabecinhas, R. Cunha, and C. Silvestre, "A trajectory tracking control law for a quadrotor with slung load," *Automatica*, vol. 106, pp. 384–389, 2019.

[5] D. Dačic, D. Nesic, and P. Kokotovic, "Path-following for nonlinear systems with unstable zero dynamics," *IEEE Trans. Automat. Contr.*, vol. 52, no. 3, pp. 481–487, 2007.

[6] L. Qiu and E. J. Davison, "Performance limitations of non-minimum phase systems in the servomechanism problem," *Automatica*, vol. 29, no. 2, pp. 337–349, 1993.

[7] M. Seron, J. Braslavsky, P. Kokotovic, and D. Mayne, "Feedback limitations in nonlinear systems: From Bode integrals to cheap control," *IEEE Trans. Automat. Contr.*, vol. 44, no. 4, pp. 829–833, 1999.

[8] P. Aguiar, D. Dačić, J. Hespanha, and P. Kokotović, "Path-following or reference tracking?: An answer relaxing the limits to performance," *IFAC Proceedings Volumes*, vol. 37, no. 8, pp. 167–172, 2004.

[9] P. Aguiar, J. Hespanha, and P. Kokotovic, "Path-following for nonminimum phase systems removes performance limitations," *IEEE Trans. Automat. Contr.*, vol. 50, no. 2, pp. 234–239, 2005.

[10] A. Aguiar, J. Hespanha, and P. Kokotović, "Performance limitations in reference tracking and path following for nonlinear systems," *Automatica*, vol. 44, no. 3, pp. 598–610, 2008.

[11] J. Hauser and R. Hindman, "Maneuver regulation from trajectory tracking: Feedback linearizable systems," *IFAC Proceedings Volumes*, vol. 28, no. 14, pp. 595–600, 1995.

[12] S. Al-Hiddabi and H. McClamroch, "Tracking and maneuver regulation control for nonlinear nonminimum phase systems: Application to flight control," *IEEE Trans. Contr. Syst. Technol.*, vol. 10, no. 6, pp. 780–792, 2002.

[13] R. Skjetne, T. Fossen, and P. Kokotović, "Robust output maneuvering for a class of nonlinear systems," *Automatica*, vol. 40, no. 3, pp. 373–383, 2004.

[14] D. Dačić and P. Kokotović, "Path-following for linear systems with unstable zero dynamics," *Automatica*, vol. 42, no. 10, pp. 1673–1683, 2006.

[15] P. Aguiar and J. Hespanha, "Trajectory-tracking and path-following of underactuated autonomous vehicles with parametric modeling uncertainty," *IEEE Trans. Automat. Contr.*, vol. 52, no. 8, pp. 1362–1379, 2007.

[16] A. Shiriaev, J. W. Perram, and C. Canudas-de Wit, "Constructive tool for orbital stabilization of underactuated nonlinear systems: Virtual constraints approach," *IEEE Trans. Automat. Contr.*, vol. 50, no. 8, pp. 1164–1176, 2005.

[17] U. Mettin, P. La Hera, D. O. Morales, A. Shiriaev, L. Freidovich, and S. Westerberg, "Path-constrained trajectory planning and time-independent motion control: Application to a forestry crane," in *Proc. IEEE Int. Conf. on Advanced Robotics*, vol. 129, 2009.

[18] M. Maggiore and L. Consolini, "Virtual holonomic constraints for Euler–Lagrange systems," *IEEE Trans. Automat. Contr.*, vol. 58, no. 4, pp. 1001–1008, 2012.

[19] M. I. El-Hawwary and M. Maggiore, "Global path following for the unicycle and other results," in *Proc. American Control Conf.*, 2008, pp. 3500–3505.

[20] O. Sørdalen and C. C. De Wit, "Path following and stabilization of a mobile robot," in *IFAC Symp. on Nonlinear Cont. Syst. Design*. Elsevier, 1992, pp. 471–476.

[21] C. Samson, "Control of chained systems application to path following and time-varying point-stabilization of mobile robots," *IEEE Trans. Automat. Contr.*, vol. 40, no. 1, pp. 64–77, 1995.

[22] A. Banaszuk and J. Hauser, "Feedback linearization of transverse dynamics for periodic orbits," *Syst. & Control Lett.*, vol. 26, no. 2, pp. 95–105, 1995.

[23] A. Hladio, C. Nielsen, and D. Wang, "Path following for a class of mechanical systems," *IEEE Trans. Contr. Syst. Technol.*, vol. 21, no. 6, pp. 2380–2390, 2012.

[24] L. Consolini, M. Maggiore, C. Nielsen, and M. Tosques, "Path following for the PVTOL aircraft," *Automatica*, vol. 46, no. 8, pp. 1284–1296, 2010.

[25] L. Qian and H. H. Liu, "Path-following control of a quadrotor UAV with a cable-suspended payload under wind disturbances," *IEEE Trans. Ind. Electr.*, vol. 67, no. 3, pp. 2021–2029, 2020.

[26] M. El-Hawwary, "Passivity methods for the stabilization of closed sets in nonlinear control systems," Ph.D. dissertation, University of Toronto, 2011.

[27] A. Akhtar, S. Saleem, and J. Shan, "Path following of a quadrotor with a cable-suspended payload," *IEEE Trans. Ind. Electr.*, 2022.
[28] J. H. Ginsberg, *Advanced Engineering Dynamics*. Cambridge University Press, 1998.
[29] M. Al Lawati, A. Mohammadhasani, Z. Jiang, and A. Lynch, "Output tracking dynamic feedback linearization of a multirotor suspended load system with disturbance robustness," *J. Intell. Robot. Syst.*, 2023, under review.
[30] C. Nielsen, C. Fulford, and M. Maggiore, "Path following using transverse feedback linearization: Application to a maglev positioning system," *Automatica*, vol. 46, no. 3, pp. 585–590, 2010.
[31] L. Consolini, M. Maggiore, M. Tosques, and C. Nielsen, "On the solution of the path following problem for the PVTOL aircraft," in *Proc. American Control Conf.*, 2009, pp. 3051–3056.
[32] M. Al Lawati and A. Lynch, "Path-following control for a unmanned aerial vehicle (UAV) slung load system," *Int. J. Control*, 2023, under review.
[33] H. K. Khalil, *Nonlinear Control*. Pearson New York, 2015.